ELSEVIER

Journal of Quantitative Spectroscopy & Radiative Transfer 86 (2004) 45–71

Journal of Quantitative Spectroscopy & Radiative Transfer

www.elsevier.com/locate/jqsrt

Two-dimensional characterization of atmospheric profile retrievals from limb sounding observations

John R. Worden[a,*], Kevin W. Bowman[a], Dylan B. Jones[b]

[a] *Jet Propulsion Laboratory, California Institute of Technology, Earth and Space Sciences Division, 4800 Oak Grove Drive, MS 183-301, Pasadena, CA 91109, USA*

[b] *Division of Engineering and Applied Sciences, Harvard University, Pierce Hall 186, 29 Oxford Street Cambridge, MA 02138, USA*

Received 20 February 2003; received in revised form 18 June 2003; accepted 8 July 2003

Abstract

Limb sounders measure atmospheric radiation that is dependent on atmospheric temperature and constituents that have a radial and angular distribution in Earth-centered coordinates. In order to evaluate the sensitivity of a limb retrieval to radial and angular distributions of trace gas concentrations, we perform and characterize one-dimensional (vertical) and two-dimensional (radial and angular) atmospheric profile retrievals. Our simulated atmosphere for these retrievals is a distribution of carbon monoxide (CO), which represents a plume off the coast of south-east Asia. Both the one-dimensional (1D) and two-dimensional (2D) limb retrievals are characterized by evaluating their averaging kernels and error covariances on a radial and angular grid that spans the plume. We apply this 2D characterization of a limb retrieval to a comparison of the 2D retrieval with the 1D (vertical) retrieval. By characterizing a limb retrieval in two dimensions the location of the air mass where the retrievals are most sensitive can be determined. For this test case the retrievals are most sensitive to the CO concentrations about 2° latitude in front of the tangent point locations. We find the information content for the 2D retrieval is an order of magnitude larger and the degrees of freedom is about a factor of two larger than that of the 1D retrieval primarily because the 2D retrieval can estimate angular distributions of CO concentrations. This 2D characterization allows the radial and angular resolution as well as the degrees of freedom and information content to be computed for these limb retrievals. We also use the 2D averaging kernel to develop a strategy for validation of a limb retrieval with an in situ measurement.

Keywords: Remote sensing; Limb sounding; Horizontal inhomogeneity; Retrieval

* Corresponding author. Tel.: +1-818-957-4458; fax: +1-818-393-4445.
E-mail address: john.worden@jpl.nasa.gov (J.R. Worden).

0022-4073/$ - see front matter © 2003 Elsevier Ltd. All rights reserved.
doi:10.1016/S0022-4073(03)00274-7

1. Introduction

A new generation of satellite instruments are in orbit or in preparation for launch that will observe the troposphere and stratosphere in order to infer atmospheric profiles of temperature and composition. These observations will provide global coverage of the troposphere and stratosphere, providing a data rich environment that will revolutionize understanding of the chemistry and dynamics of the troposphere and interactions between the troposphere and stratosphere. Many of these instruments, such as the Michelson Interferometer for Passive Atmospheric Sounding (MIPAS) aboard the European ENVISAT satellite, as well as the Tropospheric Emission Spectrometer (TES), the Microwave Limb Sounder (MLS) and the High Resolution Dynamics Limb Sounder (HIRDLS) on the Aura platform, observe the limb of the atmosphere in order to retrieve atmospheric profiles of temperature and composition.

Limb sounding of the atmosphere has distinct advantages and disadvantages over nadir (downward-looking) sounding. For example, the vertical resolution of a limb sounder can be better than that of an equivalent nadir sounder if the length scale of the sounder's field-of-view is smaller than the vertical resolution of the nadir sounder [1,2]. There is also increased sensitivity to trace gases with low atmospheric concentrations because the radiance propagates through long atmospheric path lengths before reaching the satellite [3]. On the other hand, longer path lengths may degrade the quality of a limb retrieval because of increases in opacity due to water, aerosols, and the more abundant trace gases. Long path lengths also increase the probability of cloud interference in a limb retrieval.

Limb sounding of the troposphere can be complicated because the temperature and composition of the troposphere is angularly inhomogenous due to dynamic forcing of the atmosphere. For example, Stiller et al. [4] find that temperature angular inhomogeneities can, in some instances, add errors of 100% or more to MIPAS atmospheric trace gas retrievals. Carlotti et al. [5] propose an approach that they call a "geo-fit", which simultaneously retrieves vertical profiles for an orbit of limb measurements in order to address angular inhomogeneities. Similarly Livesey and Read [6] find that temperature and gas angular inhomogeneities will affect AURA MLS retrievals. They show that a 2D retrieval of temperature and gas distribution improves the accuracy of a limb retrieval as compared to a limb retrieval that assumes an angularly homogeneous atmosphere.

In this paper we perform and evaluate 1D and 2D retrievals from a simulated limb sounding observation of a simulated distribution of carbon monoxide (CO) with angular and radial dependence. In particular, we choose a simulated plume of CO off the coast of Japan that varied from 90 to 330 ppb of CO at 5 km, over a latitude range of 10°. The radiation produced from this simulated plume of CO is used as the measurement for both the 1D and 2D limb retrieval. Characterization of these limb retrievals involves evaluating the averaging kernel and error covariance of the retrieval with respect to the radial and angular distribution of carbon monoxide. Characterizing a limb retrieval in this manner allows us to compare directly the performance of a 2D and a 1D limb retrieval of the CO plume. The averaging kernel is used to define a radial and angular resolution of the retrievals. This 2D resolution is a measure of the minimum scale length and location to which the limb retrieval is sensitive. In addition, the degrees of freedom for signal (DOFS) and the information content are computed from the averaging kernel and error covariance matrix, respectively. Specifically, we show that the DOFS and information content of the 2D limb retrieval is significantly larger than that for the 1D retrieval. The 2D characterization of a limb retrieval can also be applied to develop a strategy for validating a limb retrieval with an in situ measurement of the same air mass.

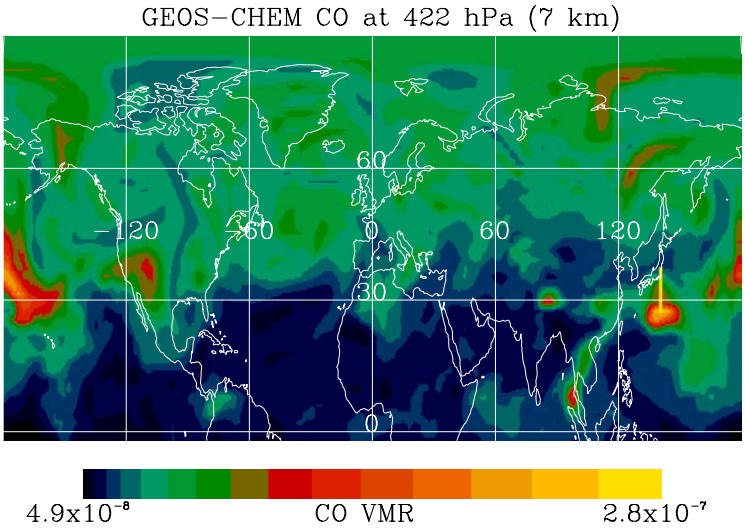

Fig. 1. GEOS-CHEM CO volume mixing ratios for model date March 25, 2001 at pressure of 422 hPa (approximately 7.0 km). This image illustrates the angular variations of CO that might be viewed by a tropospheric sounder. A bright vertical line at 30N, 140E shows the cross section of the plume used for this case study. In this simulation, TES is viewing this cross section from the North at an altitude of 705 km and at approximately 55N 140E.

2. Case study

2.1. Simulated atmosphere

We generate a simulated atmosphere consisting of profiles temperature, H_2O, O_3, and CO using the GEOS-CHEM global 3D model of tropospheric chemistry [7]. The model is driven with assimilated meteorological fields from the Goddard Earth Observing System (GEOS) of the NASA Data Assimilation Office. We employ here version 4.20 of GEOS-CHEM, which has a horizontal resolution of $2 \times 2.5^\circ$ with 48 sigma levels in the vertical from the surface to 0.01 hPa. The model includes a comprehensive treatment of O_3-NO_x-hydrocarbon chemistry in the troposphere. In the stratosphere the production rates and loss frequencies of CO are based on a stratospheric climatology derived from the Harvard 2D model [8]. Stratospheric O_3 concentrations are calculated using the linearized ozone chemistry of McLinden et al. [9].

Fig. 1 shows an image of the modeled volume mixing ratio of CO for model date March 25, 2001 at a pressure of 422 hPa (approximately 7.0 km). The modeled fields have been mapped on to the fixed pressure levels of the TES forward model by interpolating the natural logarithm of the mixing ratios as a function of the logarithm of the pressure. Fig. 1 illustrates the angular variations of carbon monoxide that are likely to be observed with tropospheric limb sounding observations. Off the coast of Japan at 30N, 140E is a plume with peak concentrations more than double the background value. A bright vertical line shows the cross section of the plume used for this case study. Fig. 2 shows the vertical CO profiles from this cross section. The black profile at 30° latitude has the largest concentrations of carbon monoxide.

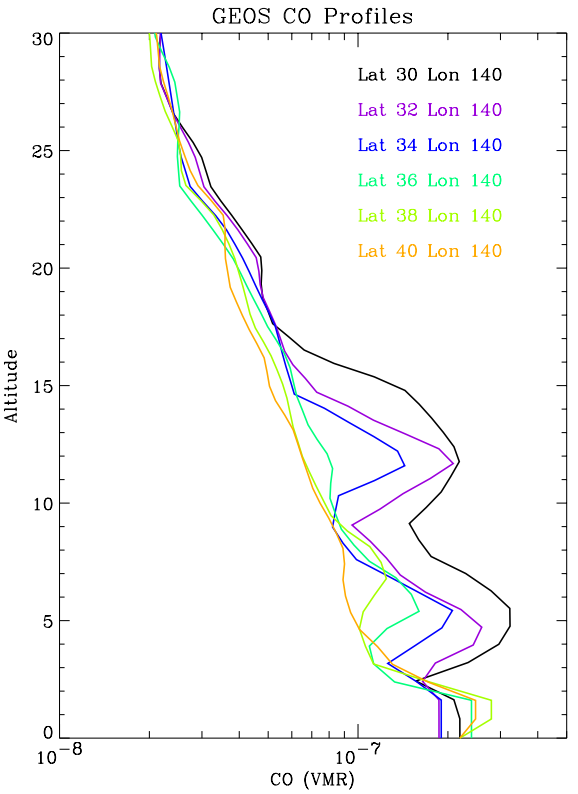

Fig. 2. Vertical CO profiles from the cross section illustrated in Fig. 1. The black profile at 30° latitude has the largest concentrations of carbon monoxide.

2.2. Tropospheric emission spectrometer

Our simulated viewing platform is the TES instrument [10], which is scheduled to launch in 2004 aboard the Earth Observing System (EOS) Aura satellite. The TES is a Fourier transform spectrometer with a spectral range between 650 and 2250 cm^{-1}. Four arrays of 16 detectors each measure the outgoing atmospheric radiance. In the limb mode, the centers of the detector arrays are pointed to approximately 16 km above the surface. The full-width-half-maximum (FWHM) for the field-of-view (FOV) of each detector is approximately 2.0 km so that the full field-of-regard (FOR) is about 32 km for the entire detector array. The FOV of a detector overlaps that of the adjacent detector near the half-width of the detector FOV. Part of the sequence of measurements taken by TES are three sequential limb scans that are within approximately 1° of each other. We therefore combine these three measurements for the 2D retrieval because the cross section of air viewed by each limb scan strongly overlaps.

2.3. Assumptions for 2D limb retrieval of carbon monoxide

The strategy for both TES nadir and limb profile retrievals is to first retrieve atmospheric temperature and H_2O, followed by ozone and then other trace gases such as CO, CH_4, HNO_3, NO, NO_2,

etc. However, in order to focus on the 2D characterization of a limb profile retrieval we retrieve only the radial and angular distribution of CO and assume that all other atmospheric quantities are known perfectly and that there are no systematic errors from either the forward model or instrument. In addition, we assume that there are no clouds and that the atmosphere is non-scattering. A future paper that characterizes the TES limb-viewing capabilities will systematically retrieve all relevant quantities (e.g., temperature and interfering species) prior to characterizing the retrieval of a species of interest.

The spectral region between 2080 and 2110 cm^{-1} is used for the retrieval of CO described in this study. The noise equivalent spectral radiance (NESR) for this spectral range is 1.7×10^{-8} W cm^{-2} sr^{-1} cm^{-1} for each detector. We include CO_2, H_2O, and O_3 as interfering species in our model atmosphere. The temperature, water, and ozone fields are also from the GEOS-CHEM model but are assumed to be angularly homogeneous for the purpose of simplifying this analysis.

3. Forward model

3.1. Forward model for an angularly homogenous atmosphere

In order to model the radiance field across the TES detectors for a homogeneous atmosphere, we follow Clough et al. [11] who summarize the calculation of the radiance field incident on the TES detectors, and the subsequent limb retrieval of ozone for a simulated, angularly homogeneous atmosphere using the expected TES instrument configuration and viewing geometry. The angularly homogenous atmosphere used for the radiative transfer, or "forward" model, in a 1D vertical retrieval is depicted in Figs. 3a and b. The atmosphere is described as a set of 86 concentric layers that are separated by 87 constant pressure surfaces or "levels" that range from 1014 to 0.01 hPa. The collection of these constant pressure surfaces constitute the radial grid. Each layer is composed of a mixture of gas that is a function of averaged pressure and temperature, denoted as $\bar{P}_k$ and $\bar{T}_k$ for layer k, respectively. The angular radiation field measured by the TES detectors is discretized with a bundle of rays that span the TES FOV. Each ray is traced through the atmosphere to the TES sensors. A simplification in this ray tracing can be made by specifying that each ray must correspond to a tangent point of one of the TES FM pressure levels; a tangent point is defined as the location where a ray is coincident and parallel to a level.

The radiance for a single ray can be described as a function of the radiance along the ray path in front of the tangent point as described in Fig. 3a and the radiance behind the tangent point:

$$L^i_{\text{ray}}(v) = L^i_{\text{back}}(v)\mathrm{T}_{i,N}(v) + L^i_{\text{front}}(v), \tag{1}$$

where i is the pressure level corresponding to the tangent point, v is the frequency of the radiance in cm^1, and N is the total number of layers in the atmosphere. The total transmittance from the tangent point at level k to the top of the atmosphere is

$$\mathrm{T}_{i,N}(v) = \prod_{k=i}^{N} \mathrm{T}_k(v), \tag{2}$$

where the transmittance for each layer i is:

$$\mathrm{T}_k(v) = \mathrm{e}^{-\tau_k(v)} \tag{3}$$

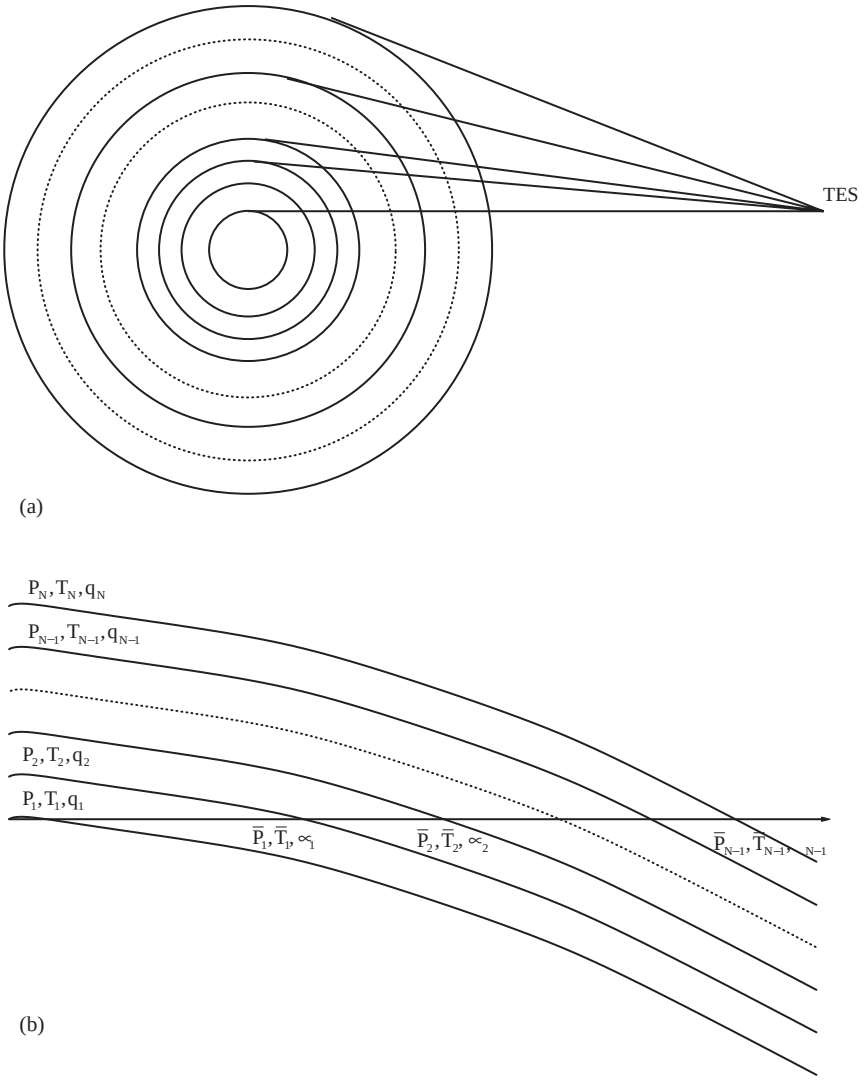

Fig. 3. (a) A depiction of rays traced from tangent points to the TES detectors. Note that this figure is not to scale. A set of rays, which are incident on the TES detectors at different angles, are used to discretize the angular radiance field observed by TES. (b) An illustration of a ray traced through a set of levels and layers for a homogenous atmosphere. Level quantities such as pressure, temperature, and mixing ratio (P, T, q) are shown on the left of the figure. Layer quantities for the ray are shown next to the ray path; layer quantities depend on the path through the layer and on the levels that bound the layer.

and the optical depth $\tau(v)$ is defined as

$$\tau_k(v) = \sum_{l=1}^{N_s} \mu_k^l \kappa^l(v, \bar{P}_k, \bar{T}_k), \tag{4}$$

where N_s is the total number of species, μ_k^l is the column amount for the kth layer and the lth species, κ_l is the absorption coefficient for the lth species, $\bar{P}_k$ is the averaged layer pressure, and $\bar{T}_k$ is the averaged layer temperature for layer k.

Layer quantities such as the column amount of each atmospheric species as well as the average pressure and temperature of the layer, depend on the pressure, temperature, and corresponding mixing ratios at the adjacent levels as illustrated in Fig. 3b. For example, the column amount in Eq. (4) can be expressed as

$$\mu_k = \mu_k(q_{\text{ray}}(P_i), q_{\text{ray}}(P_{i+1})), \tag{5}$$

where q_{ray} is the volume mixing along the ray path evaluated at pressure levels i and $i+1$. For a homogeneous atmosphere there is no angular dependence on trace gas concentrations.

The radiance for the "front" component of a ray is computed by numerically integrating thermal radiance contributions from each layer of the forward model. The radiance contribution from each layer depends on the optical thickness of each species within the layer as well as the thermal contribution as accounted for by the Planck function:

$$L_{\text{front}}^k(v) = \sum_{i=k}^{N} (1 - \mathrm{T}_i(v))B(v, \bar{T}_i)\mathrm{T}_{i+1,N}(v), \tag{6}$$

where B is the Planck function.

For the TES forward model, absorption coefficients for each species, $\kappa^l(v)$, are computed by interpolating between absorption coefficient look-up tables specified on a pre-defined pressure and temperature grid. These pre-defined absorption coefficient tables are generated using the Line-By-Line Radiation Transfer Model (LBLRTM) [12,13]. The radiative transfer approach for computing the radiance of each ray is also based on LBLRTM, that is, Eq. (6) is evaluated recursively. Note that for an angularly homogenous atmosphere, the atmosphere is symmetric with respect to the tangent point. Consequently, the "back" and "front" layer quantities are the same for each ray.

Each ray spectra is convolved with the TES instrument-line-shape (ILS) function to account for the TES spectral resolution. Then, the radiances from the bundle of rays are integrated over the angular response of each detector (i.e., the detector FOV) to compute the expected angular radiance for each of the TES detectors [11].

3.2. Ray tracing for angularly inhomogenous atmosphere

The transfer of radiation through an angularly inhomogeneous atmosphere can be computed in the same manner as for an angularly homogeneous atmosphere. However, the ray tracing approach must be modified to account for a radial and angular distribution of temperature or atmospheric constituents. Fig. 4a describes some of the salient aspects of our 2D ray tracing approach. The atmosphere must now be defined on a fixed radial and angular grid. In Fig. 4a, the angular grid is defined by interpolating the GEOS-CHEM profiles to a 1° latitudinal grid. The surface altitude is set to 0 km and the surface pressure is fixed to 1000 hPa. As with the homogeneous case, rays correspond to tangent points on pressure levels. However, the angular location of each tangent point, relative to the satellite and the fixed angular grid of the atmosphere, must also be defined. Tangent point locations are computed using the approach described by Rodgers [14].

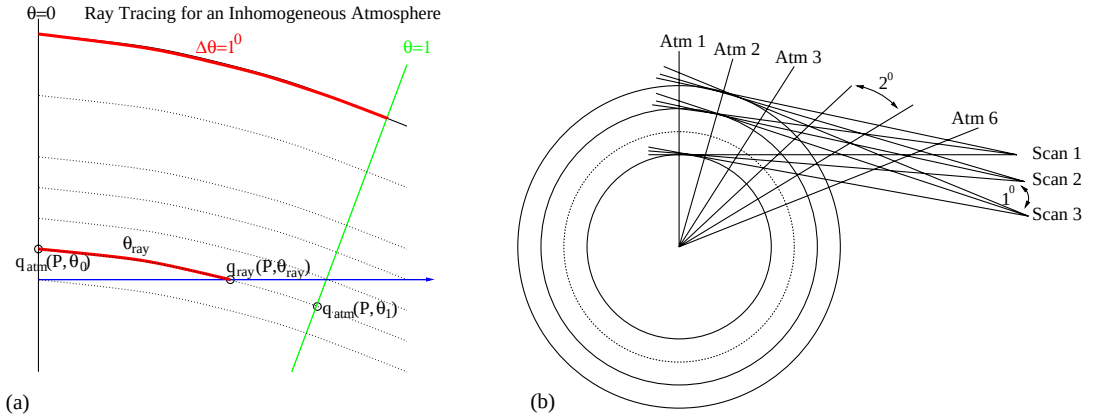

Fig. 4. (a) Limb ray tracing approach for inhomogeneous atmosphere. The mixing ratio, q_{ray}, at the point where a ray intersects a pressure level is determined by interpolating in angle between the mixing ratios that are defined on adjacent profiles. This approach is used to compute the mixing ratios along the ray path at each pressure level. (b) Viewing geometry for TES 2D retrieval. There are 6 lines, denoted by Atm 1–Atm 6, which represent vertical carbon monoxide profiles that are generated by the GEOS-CHEM model. Examples of rays traced from tangent point locations to the satellite (denoted by Scans 1–3) are depicted. The rays traced to a specific satellite location represent the field-of-view of a TES measurement. This figure illustrates how the field-of-view of these TES limb measurements overlap.

At each point where a ray intersects a TES pressure level, the volume-mixing ratio (VMR) is computed by interpolating in angle between the VMR of the gas of the two nearest profiles on the same pressure level (Fig. 4a). The calculation of this angle must also account for bending related to the index of refraction [14,15]. For example, if a ray intersects level i between profiles j and $j+1$ at an angle θ then the volume mixing ratio of the trace gas, $q_{\text{ray}}(P_i,\theta)$, at level i for the ray is

$$q_{\text{ray}}(P_i,\theta) = (1-\alpha)q(P_i,\theta_j) + \alpha q(P_i,\theta_{j+1}), \tag{7}$$

where $\theta \in [\theta_j,\theta_{j+1}]$ and the interpolation coefficient α is

$$\alpha = \begin{cases} \dfrac{\theta-\theta_j}{\theta_{j+1}-\theta_j}, & \theta_j \leqslant \theta \leqslant \theta_{j+1}, \\ 0 & \text{otherwise.} \end{cases} \tag{8}$$

The quantity θ is the zenith angle of the point where the ray intersects a pressure level. The quantities θ_j and θ_{j+1} are the zenith angles of the two nearest profiles. In this manner, a set of mixing ratios, defined on the TES fixed pressure grid, is computed for each ray that accounts for the radial and angular distribution of the atmosphere. Layer quantities such as column amounts, average pressure, and average temperature are computed using these interpolated mixing ratios.

3.3. Jacobians

The TES forward model and retrieval algorithm analytically computes the derivative (or Jacobian) of the ray radiance with respect to the natural log of the VMR at each pressure P_i and each angle θ_j.

The Jacobian for the ray radiance can be written as

$$K_{\text{ray}}(v, \ln q(P_i, \theta_j)) = \frac{\partial L_{\text{ray}}(v)}{\partial \ln q(P_i, \theta_j)} = \frac{\partial L_{\text{ray}}(v)}{\partial \ln q_{\text{ray}}(P_i, \theta)} \frac{\partial \ln q_{\text{ray}}(P_i, \theta)}{\partial \ln q(P_i, \theta_j)}. \tag{9}$$

The Jacobian in Eq. (9) is expanded into a product of two terms. The first term, $\partial L_{\text{ray}}(v)/\partial \ln q_{\text{ray}}(p_i, \theta_j)$, of the Jacobian is computed from Eq. (6). A description of this part of the analytic Jacobian is beyond the scope of this paper. The second term $\partial \ln q_{\text{ray}}(P_i, \theta)/\partial \ln q(P_i, \theta_j)$ is expanded into the following:

$$\frac{\partial \ln q_{\text{ray}}(P_i, \theta)}{\partial \ln q(P_i, \theta_j)} = \frac{q(P_i, \theta_j)}{q_{\text{ray}}(P_i, \theta)} \frac{\partial q_{\text{ray}}(P_i, \theta)}{\partial q(P_i, \theta_j)}, \tag{10}$$

where

$$\frac{\partial q_{\text{ray}}(P_i, \theta)}{\partial q(P_i, \theta_j)} = (1 - \alpha), \tag{11}$$

$$\frac{\partial q_{\text{ray}}(P_i, \theta)}{\partial q(P_i, \theta_{j+1})} = \alpha \tag{12}$$

are computed by differentiating Eq. (7). Eq. (9) is used to map a ray Jacobian, evaluated with respect to the mixing ratios along the ray path, q_{ray}, to a ray Jacobian that is evaluated on the full pressure and angular grid.

As with the radiance, the collection of ray Jacobians on the 2D grid are first convolved with the TES instrument-line-shape function. Then the ray Jacobians for each profile are integrated over the angular response of each of the TES detectors to obtain a set of detector Jacobians over the full, fixed pressure and angular grid.

4. Estimation theory

Measured radiances in TES can be related to a forward model through the following additive noise model:

$$\mathbf{y} = \mathbf{F}(\mathbf{x}, \mathbf{b}; v) + \mathbf{n}, \tag{13}$$

where $y \in \mathbb{R}^N$ is the observation vector containing the calibrated, measured spectra. The observation vector is the sum of the non-linear forward model operator, $\mathbf{F} : \mathbb{R}^M \rightarrow \mathbb{R}^N$, which simulates a spectrum produced from the propagation of radiation through the atmosphere to the spacecraft, and the noise term $\boldsymbol{n} \in \mathbb{R}^N$, which is assumed to be zero-mean, white Gaussian noise so that:

$$\mathbf{S}_n = E[\mathbf{n}\mathbf{n}^{\mathrm{T}}] = \sigma^2 \mathbf{I}, \tag{14}$$

where $E[\cdot]$ is the expectation operator [16] and σ^2 is the variance of the noise. The forward model is a function of the "full" state vector, $\mathbf{x} \in \mathbb{R}^M$ where $\mathbf{x}$ is the distribution of the retrieved atmospheric gas. For example, in this study the full state vector $\mathbf{x}$ is the log of the volume mixing ratio (vmr) of carbon monoxide as a function of log pressure grid (P) and angle (θ). For the carbon monoxide

plume, the full state vector is discretized on $N = 85$ pressure levels and $L = 12$ angles:

$$\mathbf{x} = \ln \begin{bmatrix} q(P_0, \theta_1) \\ \vdots \\ q(P_N, \theta_1) \\ \vdots \\ q(P_0, \theta_L) \\ \vdots \\ q(P_N, \theta_L) \end{bmatrix}. \tag{15}$$

The vector **b** contains all the other parameters, trace gases, atmospheric temperature distribution, geometry of the spacecraft, etc., necessary to define the angular radiance for the TES sensors. The vector **b** will be dropped in subsequent derivations because these parameters are fixed for the purpose of simplifying this study. Fine discretization in both pressure and angle is required to model accurately the radiative transfer through the atmosphere. However, radial and angular structure present in the full state vector cannot typically be resolved on this fine grid; the retrieval must therefore be regularized. Regularization of the retrieval includes defining a retrieval vector that limits the possible values of the full state vector. For this study, the retrieval vector and the full state vector are related by a linear mapping:

$$\mathbf{x} = \mathbf{M}\mathbf{z}, \tag{16}$$

where $\mathbf{z} \in \mathbb{R}^M$ is the retrieval vector and $\mathbf{M} \in \mathbb{R}^{M \times N}$ is a mapping matrix. The mapping matrix may also be interpreted as

$$\mathbf{M} = \frac{\partial \mathbf{x}}{\partial \mathbf{z}}. \tag{17}$$

The mapping matrix represents a "hard constraint" because the estimate cannot take on values outside the range space of **M** [2,14].

The 2D retrieval can be described by the following augmented non-linear least squares (NLLS) solution:

$$\hat{\mathbf{x}} = \mathbf{M} \cdot \min_z (\|\mathbf{y} - \mathbf{F}(\mathbf{M}\mathbf{z})\|^2_{S_n^{-1}} + \|\mathbf{z} - \mathbf{z}_c\|^2_{\Lambda}), \tag{18}$$

where $\mathbf{z}_c$ is a constraint vector, $\mathbf{\Lambda} \in \mathbb{R}^{M \times M}$ is a constraint matrix and $\mathbf{S}_n$ is the error covariance matrix defined in Eq. (14). The constraint vector and matrix are referred to as "soft" constraints because they provide a priori information about the solution space, e.g., smoothness of the profile or statistical distribution of the state vector, without restricting that solution space for the estimate. The non-linear retrieval of the CO distribution is based on the iterative minimization of the observed limb radiances with the forward model evaluated at successive estimates of the CO retrieval vector.

4.1. Linear retrieval

If the estimate of carbon monoxide is "close" to the true state, then its dependence on the choice of constraint vector, constraint matrix, and true state can be described by the linear retrieval [14]

$$\hat{\mathbf{x}} = \mathbf{x}_c + \mathbf{A}_{xx}(\mathbf{x} - \mathbf{x}_c) + \mathbf{M}\mathbf{G}_z\mathbf{n}, \tag{19}$$

where $\mathbf{M}$ is the mapping matrix, $\mathbf{A}_{xx}$ is the averaging kernel matrix, $\mathbf{n}$ is the noise vector, $\mathbf{x}$ is the true full state vector (the CO distribution), $\mathbf{x}_c = \mathbf{M}\mathbf{z}_c$ is the constraint state vector, and $\mathbf{G}_z$ is the gain matrix, which is defined by

$$\mathbf{G}_z = \frac{\partial \mathbf{z}}{\partial \mathbf{F}} = (\mathbf{K}_z{}^{\mathrm{T}}\mathbf{S}_n^{-1}\mathbf{K}_z + \Lambda_z)^{-1}\mathbf{K}_z{}^{\mathrm{T}}\mathbf{S}_n^{-1}. \tag{20}$$

The retrieval Jacobian, $\mathbf{K}_z$, is defined by

$$\mathbf{K}_z = \frac{\partial \mathbf{F}}{\partial \mathbf{x}}\frac{\partial \mathbf{x}}{\partial \mathbf{z}} = \mathbf{K}_x\mathbf{M}. \tag{21}$$

Eq. (19) is a valid approximation to Eq. (18) when

$$\mathbf{K}_x(\mathbf{x} - \hat{\mathbf{x}}) \approx \mathbf{F}(\mathbf{x}, \mathbf{b}) - \mathbf{F}(\hat{\mathbf{x}}, \mathbf{b}), \tag{22}$$

where $\mathbf{F}$ is defined in Eq. (9).

The averaging kernel matrix or resolution matrix, $\mathbf{A}_{xx} = \partial\hat{\mathbf{x}}/\partial\mathbf{x}$ is the sensitivity of the retrieval to the true state of the atmosphere [14] and is computed by the following equation:

$$\mathbf{A}_{xx} = \frac{\partial \hat{\mathbf{x}}}{\partial \mathbf{x}} = \frac{\partial \hat{\mathbf{x}}}{\partial \mathbf{z}}\frac{\partial \mathbf{z}}{\partial \mathbf{F}}\frac{\partial \mathbf{F}}{\partial \mathbf{x}} = \mathbf{M}\mathbf{G}_z\mathbf{K}_x. \tag{23}$$

The resolution of the retrieval can be derived from the columns of the averaging kernel matrix, $\partial\hat{\mathbf{x}}_i/\partial\mathbf{x}$, which define the relative contribution of each element of the true state to the estimate at a particular pressure and angle. In many cases, the elements of the true state that have the greatest contribution to the estimate are also in close proximity to the estimate. In those cases, the resolution can be defined as the "width" or "area" of the subset of elements of the true state that have a relative contribution greater than some threshold [17]. The resolution for a 2D retrieval will be described in more detail in Section 5.

When the constraint vector and matrix are the mean and covariance of the state vector, then the DOFS of the retrieval can be calculated from the averaging kernel matrix [14]:

$$\mathrm{DOFS} \triangleq \mathrm{tr}[\mathbf{A}_{xx}]. \tag{24}$$

The degrees of freedom for signal of the retrieval may be interpreted as the number of statistically independent elements of the estimate.

4.2. Error analysis

The error in the estimate of the atmospheric profile is the true state minus the estimate:

$$\tilde{\mathbf{x}} = \mathbf{x} - \hat{\mathbf{x}}. \tag{25}$$

Substituting Eq. (19) into Eq. (25) leads to

$$\tilde{\mathbf{x}} = \underbrace{(\mathbf{I} - \mathbf{A}_{xx})(\mathbf{x} - \mathbf{x}_c)}_{\text{smoothing error}} + \underbrace{\mathbf{M}\mathbf{G}_z\mathbf{n}}_{\text{noise error}}. \tag{26}$$

The right-hand side of this equation is composed of two terms. The second term transforms the random spectral error to an error on the full state vector. The first term results from applying constraints to the estimate of ozone on this specific grid. These constraints can be a combination of "hard" constraints, e.g. representing the profile on a coarse pressure grid, or "soft" constraints, e.g. adding a quadratic penalty function in Eq. (20) to ensure an acceptable regularization. This term is the so-called "smoothing" error [14]. Physically, the smoothing error describes the extent to which a remote observing system is sensitive to fine structure as defined, in this context, on the forward model grid.

The mean of the error vector defined on the full-state grid is

$$E[\tilde{\mathbf{x}}] = (\mathbf{I} - \mathbf{A}_{xx})(\bar{\mathbf{x}} - \mathbf{x}_c), \tag{27}$$

where $\bar{\mathbf{x}} = E[\mathbf{x}]$. We have assumed a zero-mean measurement noise vector for Eq. (24). The total error covariance matrix is

$$\mathbf{S}_{\tilde{x}} = (\mathbf{A}_{xx} - \mathbf{I})\mathbf{S}_a(\mathbf{A}_{xx} - \mathbf{I})^{\mathrm{T}} + \mathbf{M}\mathbf{G}_z\mathbf{S}_n\mathbf{G}_z^{\mathrm{T}}\mathbf{M}^{\mathrm{T}}, \tag{28}$$

where $\mathbf{S}_{\tilde{x}} = E[(\tilde{\mathbf{x}} - \bar{\tilde{\mathbf{x}}})(\tilde{\mathbf{x}} - \bar{\tilde{\mathbf{x}}})^{\mathrm{T}}]$, $\bar{\tilde{\mathbf{x}}} = E[\tilde{\mathbf{x}}]$, and $\mathbf{S}_a = E[(\mathbf{x} - \bar{\mathbf{x}})(\mathbf{x} - \bar{\mathbf{x}})^{\mathrm{T}}]$. The smoothing error covariance matrix is composed of the averaging kernel matrix and the covariance of the state vector. Hence, the smoothing error will decrease as the resolution of the retrieval increases, i.e., the averaging kernel matrix will approximate the identity matrix, or if there is little variance in the state vector.

We base the a priori statistics of the state vector on a 2D climatological covariance that is constructed in part from the GEOS-CHEM model. First, a 1D climatological covariance matrix is computed from the GEOS-CHEM (Section 2.1) model for the region between 57° and 177°E longitude and 20° through 60°N latitude so that

$$\mathbf{S}_a^{1\mathrm{D}} = E[(\mathbf{x}_{1\mathrm{D}} - \bar{\mathbf{x}}_{1\mathrm{D}})(\mathbf{x}_{1\mathrm{D}} - \bar{\mathbf{x}}_{1\mathrm{D}})^{\mathrm{T}}], \tag{29}$$

where $\mathbf{x}_{1\mathrm{D}}$ is the vertical full state vector for one angle. For simplicity, we assume that the covariance for all profiles is equal to the 1D covariance.

The 2D climatological covariance matrix is constructed by first creating a block diagonal matrix where each sub-matrix is the covariance in Eq. (29):

$$[\mathbf{S}_a^{2\mathrm{D}}]_{ii} = S_a^{1\mathrm{D}}, \tag{30}$$

where the indices ii refer to the block diagonal components of $\mathbf{S}_a^{2\mathrm{D}}$. This 2D climatological covariance, $\mathbf{S}_a^{2\mathrm{D}}$, is used for S_a in Eq. (28). For simplicity we introduce an ad hoc exponential correlation between profiles in the off-diagonal blocks of the matrix:

$$[\mathbf{S}_a^{2\mathrm{D}}]_{ij} = \mathrm{e}^{-|i-j|}\mathbf{S}_a^{1\mathrm{D}}, \tag{31}$$

where the indices i and j refer to the off-diagonal blocks of the matrix $\mathbf{S}_a^{2\mathrm{D}}$.

A measure of the performance of the retrieval is the "information content" [14], which is defined as

$$\Delta \mathbf{H} = \frac{1}{2}\log_2\left(\frac{|\mathbf{S}_a|}{|\mathbf{S}_{\hat{\mathbf{x}}}|}\right) = \frac{1}{2}(\log_2|\mathbf{S}_{\mathrm{a}}| - \log_2|\mathbf{S}_{\hat{\mathbf{x}}}|), \tag{32}$$

where $|\cdot|$ is the determinant operator. The determinant of the total error covariance matrix defines the total error volume for the covariance. Likewise, the determinant of the covariance matrix of the atmospheric constituent, which is defined by $\mathbf{S}_a$, is a measure of the volume of uncertainty of that constituent. The information content therefore describes the relative increase in "knowledge", i.e., decrease in error volume, relative to the a priori knowledge of the atmospheric state. The unit of information content in Eq. (32) is *bits*. The information content increases by one bit for every factor of two decrease in error volume relative to the volume of uncertainty of the atmospheric state.

5. Carbon monoxide limb retrieval

5.1. TES viewing geometry

The TES takes 3 limb measurements, separated by 1°, as part of the standard survey mode that also includes nadir measurements and calibration. These 3 limb measurements are combined because the FOV of these measurements overlap. The geometry for combining the 3 TES limb scans is illustrated in Fig. 4b. Six GEOS-CHEM carbon monoxide profiles span the CO plume and the TES FOV of the combined measurements. The profiles of the atmosphere at angles behind the reference profile are set to a priori values because contribution of the radiance from these profiles to the radiance measured at the satellite is negligible. In order to better characterize the angular resolution of TES, the six GEOS profiles, spaced every 2° latitude are interpolated to 12 profiles, spaced every 1° latitude.

Section 3.3 discusses how the Jacobians for each detector of each of the TES measurements are computed for this set of profiles. The set of 16 detector Jacobians from each of the TES measurements are stacked together in the following manner:

$$\mathbf{K}_x = \begin{bmatrix} \mathbf{K}_{\mathrm{det1}}^{\mathrm{scan1}} \\ \vdots \\ \mathbf{K}_{\mathrm{det16}}^{\mathrm{scan1}} \\ \vdots \\ \mathbf{K}_{\mathrm{det1}}^{\mathrm{scan3}} \\ \vdots \\ \mathbf{K}_{\mathrm{det16}}^{\mathrm{scan3}} \end{bmatrix} \tag{33}$$

where the subscript "det" refers to detector and the superscript "scan" refers to each of the limb sounding measurements.

5.2. Mapping for 2D retrieval

Vertical retrieval levels are defined on a subset of the forward model pressure levels of each profile. The map that we use to connect retrieval levels to forward model levels is two-point linear interpolation as a function of log pressure. For a single profile with forward model levels i and retrieval levels j, this map is a matrix $\mathbf{M} \in \mathbb{R}^{M \times N}$ whose elements are defined as

$$\mathbf{M}_{ij} = \begin{cases} 1 - \dfrac{\ln P_i - \ln P_j}{\ln P_{j+1} - \ln P_j} & (P_j \leqslant P_i \leqslant P_{j+1}), \\ 0 & \text{otherwise.} \end{cases} \tag{34}$$

Vertical retrieval levels are specified to coincide with every other pressure level on the forward model grid in the troposphere but with coarser representation in the stratosphere such that there are 25 retrieval levels total.

The matrix that maps the 2D retrieval vector to the 2D full state vector is block diagonal and therefore angularly independent:

$$\mathbf{M}_v = \begin{pmatrix} \mathbf{M} & & 0 \\ & \ddots & \\ 0 & & \mathbf{M} \end{pmatrix}, \tag{35}$$

where $\mathbf{M}$ is defined in Eq. (34). The relationship between the full state vector and retrieval vector can be described by substituting Eqs. (15) and (35) into Eq. (16):

$$\mathbf{x} = \ln \begin{bmatrix} q(P_0, \theta_1) \\ \vdots \\ q(P_N, \theta_1) \\ \vdots \\ q(P_0, \theta_L) \\ \vdots \\ q(P_N, \theta_L) \end{bmatrix} = \mathbf{M}_v \ln \begin{bmatrix} q_z(P_0, \theta_1) \\ \vdots \\ q_z(P_M, \theta_1) \\ \vdots \\ q_z(P_0, \theta_L) \\ \vdots \\ q_z(P_M, \theta_L) \end{bmatrix}. \tag{36}$$

On the right-hand side of Eq. (36), the subscript $\mathbf{z}$ refers to the vertical retrieval levels and M is the number of retrieval levels for a profile. The 2D retrieval Jacobian is calculated by substituting Eqs. (33) and (35) into Eq. (21):

$$\mathbf{K}_z^{2D} = \mathbf{K}_x^{2D} \mathbf{M}_v. \tag{37}$$

5.3. Constraint selection

The constraint used for this retrieval is based on the inverse of a 2D climatological covariance described in Eqs. (30) and (31). This 2D climatology on the full-state grid is mapped to the 2D

retrieval grid using a least-squares inverse of Eq. (35):

$$\mathbf{M}_v^* = (\mathbf{M}_v^{\mathrm{T}}\mathbf{M}_v)^{-1}\mathbf{M}_v^{\mathrm{T}}, \tag{38}$$

which results in

$$\mathbf{S}_z^{2\mathrm{D}} = \mathbf{M}_v^*\mathbf{S}_x^{2\mathrm{D}}\mathbf{M}_v^{*\mathrm{T}}. \tag{39}$$

The constraint used for the linear retrieval is simply

$$\Lambda_z = (\mathbf{S}_z^{2\mathrm{D}})^{-1}. \tag{40}$$

The CO profile at 11° from the reference profile is chosen to generate the constraint vector $\mathbf{x}_c$ because this profile is assumed to be representative of background CO concentrations. This profile is also stacked as in Eq. (15) in order to form the constraint vector.

5.4. 2D retrieval results

The 2D linear retrieval for the CO plume is computed by first substituting the Jacobian from Eq. (37), the constraint from Eq. (40), and the measurement error covariance from Eq. (14) into Eq. (20). The Jacobian is evaluated over the true full state vector, which is the set of profiles that span the CO plume. The standard deviation of the measurement error covariance matrix is the NESR described in Section 2.3. This gain matrix in Eq. (20) is used to calculate the averaging kernel matrix (Eq. (23)). Finally the estimate for the CO plume is calculated from Eq. (19) using the averaging kernel matrix, gain matrix, true full state vector, the constraint vector (Section 5.3), and a realization of the noise that is consistent with the NESR.

The true state, estimate, and a priori vector are shown in Fig. 5 as a function of vertical and angular coordinates. The GEOS-CHEM distribution of CO (or true full state vector) is shown in Fig. 5a as an image. The profile at 0° corresponds to the GEOS-CHEM profile at 30N 140E from Fig. 2. There are 12 profiles total, each separated by 1° in latitude. The CO concentrations between profiles are computed by interpolating between adjacent profiles. The a priori constraint vector is shown in Fig. 5b. The estimate from the 2D retrieval is shown in Fig. 5c. For the region between 0° and 1° and between 6° and 11° the estimate shows little change from the a priori. Between 2° and 5° the estimate shows enhanced CO concentrations above 6 km. Furthermore, between 2° and 5°, both the estimate and the plume decrease with angle. The estimate for all profiles follows the a priori constraint below 5 km.

5.5. 2D characterization

The 2D retrieval can be understood by examining the averaging kernel and error covariance matrices. Elements of the averaging kernel matrix describe the sensitivity of the retrieval to the true state of the atmosphere. The diagonal of the averaging kernel for the 2D retrieval, as a function of radial and angular coordinates, is shown in Fig. 6a. The retrieval is most sensitive to the true state between 6 and 13 km and between 2° and 6°. However, peak CO concentrations correspond to the tangent layers between 0° and 1.5° (see Fig. 5a). The retrieval is not sensitive to these large concentrations of CO because of the increased opacity from ozone and water (particularly the water continuum) in the tangent layers. Fig. 6a shows that the 2D retrieval is most sensitive to the

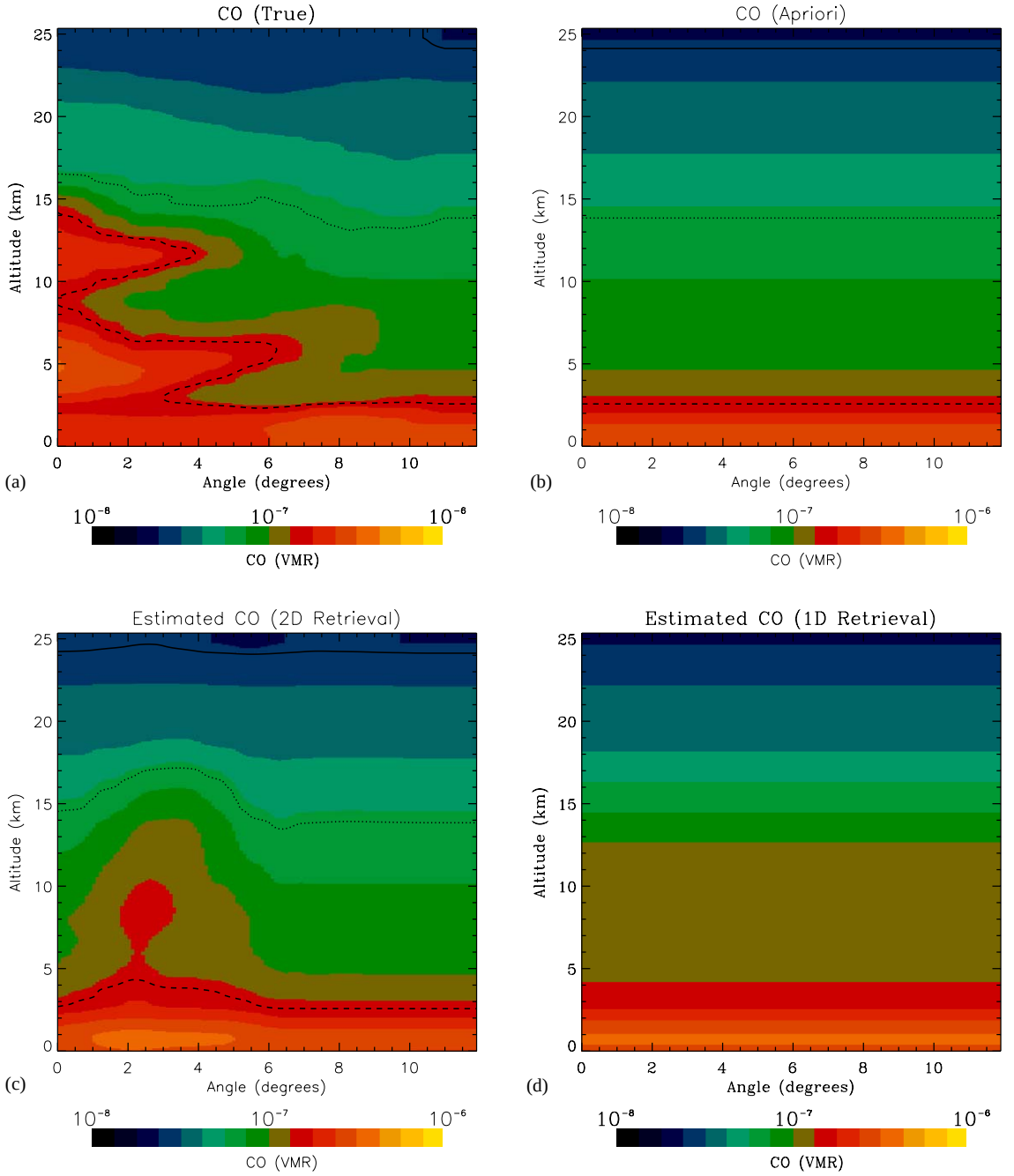

Fig. 5. (a) Distribution of CO from Fig. 2 (True). The profile at the origin of the x-axis corresponds to the profile at 30N 140E from Fig. 2. There are 12 profiles total each separated by 1° in latitude. CO amounts between profiles are interpolated from adjacent profiles. (b) Constraint vector used for the 2D and 1D limb retrieval, mapped to vertical and angular coordinates (a priori). (c) Results of the 2D retrieval and Fig. 5(d) results from the 1D retrieval.

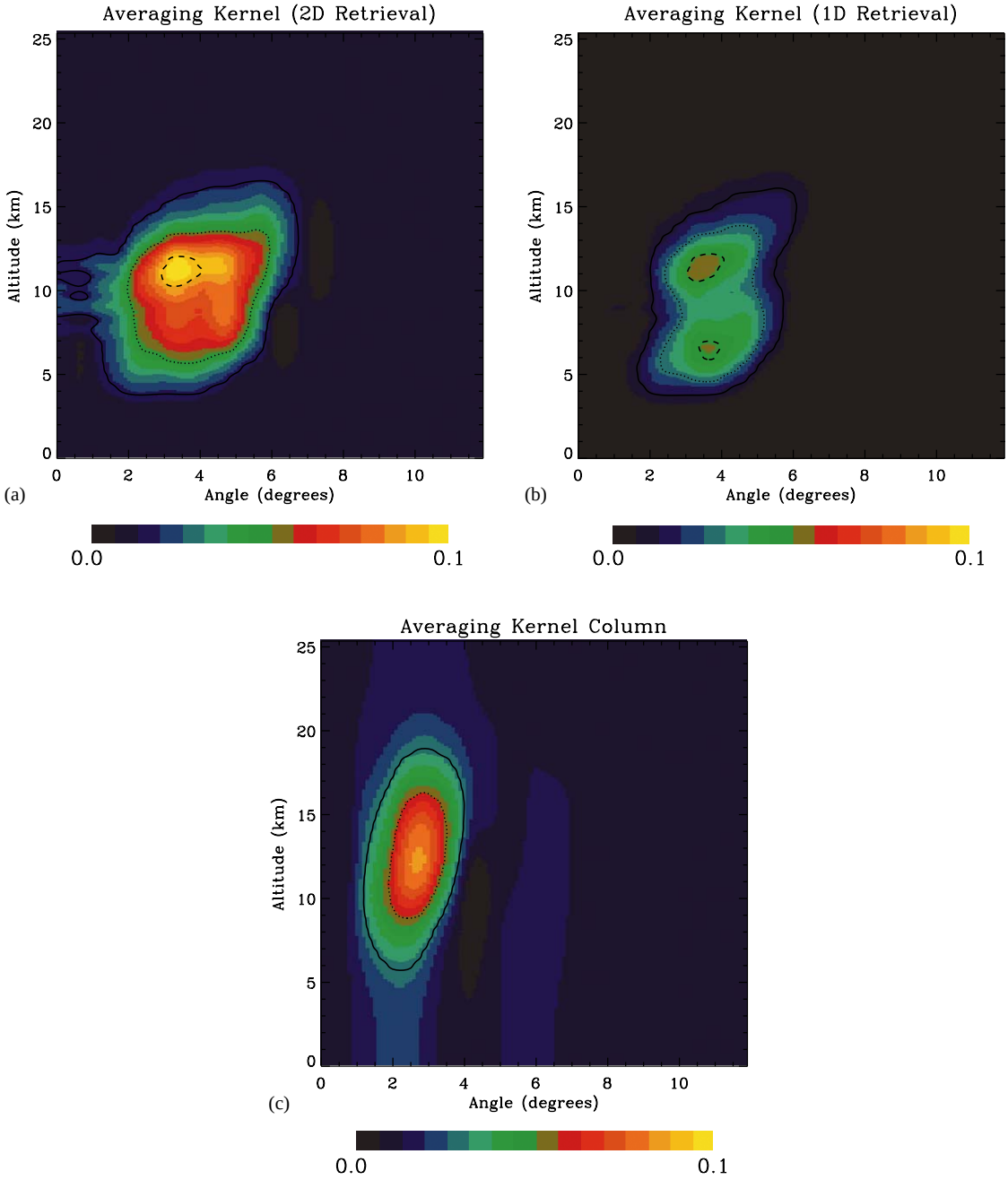

Fig. 6. (a) Diagonal elements of the averaging kernel matrix from the 2D retrieval. This diagonal of the averaging kernel, which is mapped to vertical and angular coordinates, shows where the retrieval is most sensitive to the true CO distribution. Fig. 6b shows the diagonal of the averaging kernel from the 1D retrieval. Fig. 6c shows the column of the averaging kernel matrix from the 2D retrieval that corresponds to the sensitivity of the retrieval vector at 3° and 12.4 km to the true CO distribution. The column vector of the averaging kernel is used to define the vertical and angular resolution of the 2D retrieval.

volume of air between 2° and 6°. This increased sensitivity is related to the decreased opacity from interfering species and because each of the three limb measurements view this volume of air.

The averaging kernel matrix for the 2D retrieval can also be used to describe a radial and angular resolution. This resolution can be defined from the column of the averaging kernel, $\mathbf{A}_i = \partial \hat{x}_i / \partial \mathbf{x}$, which describes how the estimate for a parameter $\hat{x}_i$ is affected by a perturbation of parameter of the true state. Fig. 6c shows the column of the averaging kernel in radial and angular coordinates, corresponding to pressure level 17 (12.4 km) for the profile at 3° from the reference. Contours on the image show where the averaging kernel is at 95%, 50%, and 10% of the maximum value of the averaging kernel column (~ 0.1). The half-width, i.e., the contour corresponding to 50% of the maximum value can be used to define a "resolution" for this retrieval at this specific level. The angular extent of the half-width, that is, the maximum angular value of the half-width minus the minimum angular value is about 1.3° and the vertical extent of the half-width is about 7 km. These resolutions are consistent with our results in that the retrieval appears to capture angular variations of the plume but only infers an average of the vertical "double peak" feature that is apparent in each of the CO profiles.

The square root of the diagonal components of the climatological covariance matrix (Eq. (29)) is shown in Fig. 7a. The square root of the diagonal elements of the total error covariance matrix (Eq. (28)) for the retrieval is shown in Fig. 7b. The total error includes the smoothing error and the noise related error (Eq. (28)). As expected, the error decreases in the region where the retrieval is sensitive as shown in Fig. 6. Fig. 7b shows that the uncertainty in CO for the volume of air between 3° and 5° latitude and between 6 and 12 km has been reduced from approximately 25% to about 10%.

5.6. Column amounts

The resolution of 1.3° and 7 km, computed from the averaging kernel, suggests that we can probably infer an integrated column for several of the profiles that span the carbon monoxide plume. For a single profile we can define a column operator that integrates the CO densities into a column amount:

$$\mathbf{c} = \mathbf{h}^{\mathrm{T}} \mathbf{x}_{1\mathrm{D}}, \tag{41}$$

where $\mathbf{h}$ is the 1D column operator that integrates the CO densities of a single profile $\mathbf{x}_{1\mathrm{D}}$ over a specified altitude range. The columns of CO for all of the profiles are calculated by

$$\mathbf{c} = \mathbf{H}\mathbf{x}, \tag{42}$$

where $\mathbf{c} \in \mathbb{R}^L$ is the CO column vector and $\mathbf{H} \in \mathbb{R}^{L \times N}$ is the column operator for all L profiles. The column operator, $\mathbf{H}$, is constructed by stacking $\mathbf{h}$ in the same manner that the 1D map is stacked in Eq. (35). The result of using the 2D column operator in Eq. (42) on the full state grid over all pressure and angles is a vector of columns for the 12 latitudinal angles. The total error of this vector of column amounts is then

$$\mathbf{S}_{\hat{c}} = \mathbf{H}\mathbf{S}_{\hat{x}}\mathbf{H}^{\mathrm{T}}, \tag{43}$$

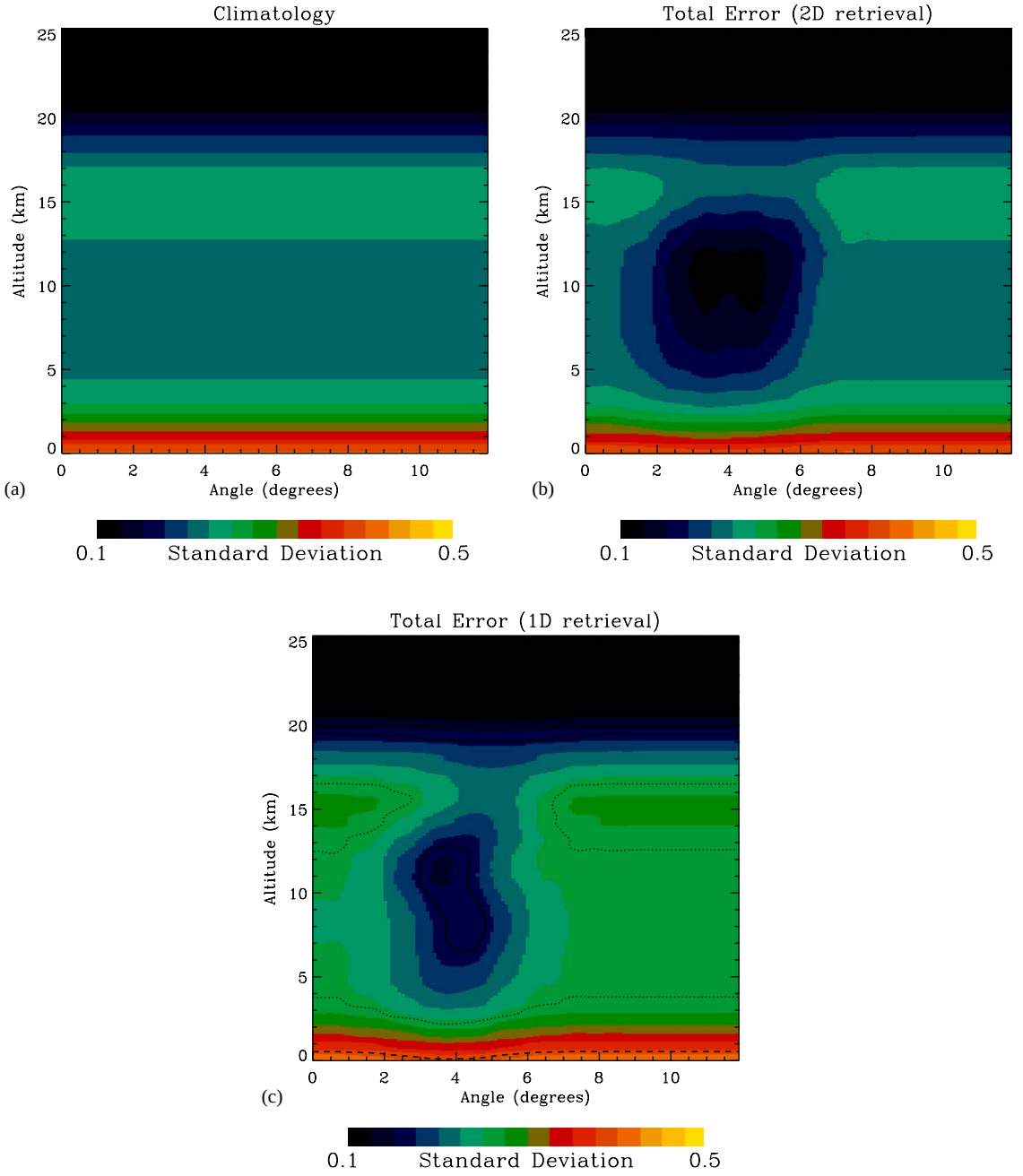

Fig. 7. Standard deviation (square root of the diagonal) of a 2D climatological covariance matrix generated from GEOS-CHEM. Fig. 7b is the standard deviation of the total error for the 2D retrieval. Fig. 7c is the standard deviation of the total error for the 1D retrieval.

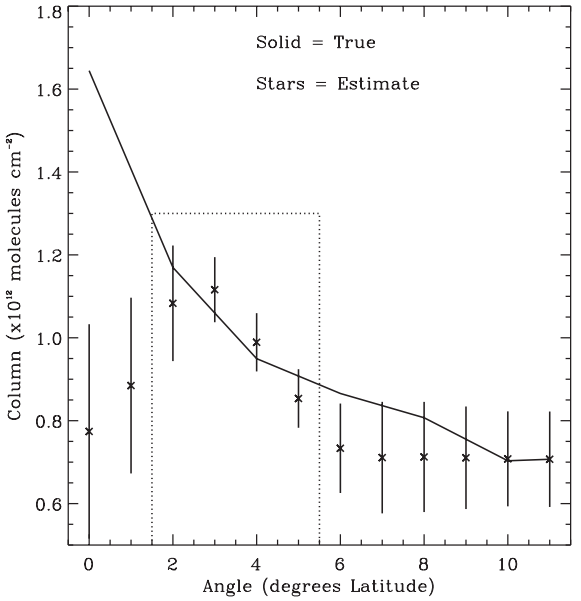

Fig. 8. Integrated column amounts for each of the vertical CO profiles that span the plume. The solid line shows the column amount for the "true" profiles and the symbols with error bars show the column amounts for the estimated profiles. The dotted rectangle shows the angular region where the retrieval is most sensitive to the CO plume.

where $\mathbf{S}_{\hat{c}} \in \mathbb{R}^{L\times L}$ is the error covariance of the column amounts and $\mathbf{S}_{\tilde{x}}$ is the total error covariance in Eq. (28) for the 2D retrieval. Because the 2D estimate is not sensitive to CO concentrations below 6 km we start the integration of the column densities above 6 km for each profile; this approach ensures that the integrated columns are minimally affected by the choice of a priori constraint. Fig. 8 shows the column amounts corresponding to each of the 12 profiles. The error bars represent the square root of the diagonal values of the $\mathbf{S}_c$ matrix. Fig. 8 shows that we can infer, within error, the integrated carbon monoxide columns for the profiles between 2° and 5° latitude from the reference with some information about the column amount for the profiles at 1° and 6° from the reference. The a priori column variance calculated from the 1D climatological covariance matrix in Eq. (29) is about 15%. What is particularly striking is that integrated columns and their angular variation between 2° and 5° from the 2D retrieval agree with the integrated columns related to the CO plume's biomass burning signature.

6. 1D limb retrieval

For a 1D retrieval, an angularly homogeneous atmosphere is used to describe the state of the atmosphere viewed by a limb sounder [11,18–20]]. This assumption of an angularly homogeneous atmosphere is reasonable for the stratosphere [21] except for example at the polar vortex [22]. For retrievals of the troposphere, the effect of angular inhomogeneity needs to be considered.

6.1. Mapping for 1D retrieval

The 1D retrieval is based on constraining the vertical profile to be the same for all angles. This constraint is implemented with a mapping matrix. The retrieval vector for the 1D retrieval is mapped to the full 2D state vector using Eq. (16) and the following mapping matrix:

$$\mathbf{M}_\theta = \begin{array}{c} \begin{array}{cccc} 1 & 2 & \cdots & M \end{array} \\ \begin{pmatrix} 1 & 0 & \cdots & 0 \\ 0 & 1 & \cdots & 0 \\ \vdots & \vdots & \vdots & \vdots \\ 0 & 0 & \cdots & 1 \\ 1 & 0 & \cdots & 0 \\ 0 & 1 & \cdots & 0 \\ \vdots & \vdots & \vdots & \vdots \\ 0 & 0 & \cdots & 1 \\ \vdots & \vdots & \vdots & \vdots \end{pmatrix} \end{array} \begin{array}{c} 1 \\ 2 \\ \vdots \\ M \\ 1 \\ 2 \\ \vdots \\ M \\ \vdots \end{array}. \tag{44}$$

The Jacobian for the 1D retrieval is calculated by substituting the Jacobian from Eq. (37) and Eq. (44) into Eq. (21). Note that this map is equivalent to summing the elements of the 2D Jacobian over angles:

$$\mathbf{K}_z^{1D} = \frac{\partial \mathbf{L}(v)}{\partial \mathbf{z}(P_i)} = \sum_i \frac{\partial \mathbf{L}(v)}{\partial \mathbf{z}(P_i, \theta_j)} = \mathbf{K}_z^{2D}\mathbf{M}_\theta. \tag{45}$$

The product of the matrix in Eq. (35) and the matrix in Eq. (44) is a single map that converts the Jacobian on the 2D full state grid to the 1D Jacobian on retrieval levels:

$$\mathbf{K}_z^{1D} = \mathbf{K}_x^{2D}\mathbf{M}_c, \tag{46}$$

where

$$\mathbf{M}_c = \mathbf{M}_v\mathbf{M}_\theta. \tag{47}$$

6.2. Constraint selection for 1D retrieval

The constraint used for the 1D retrieval is the inverse of the 1D climatological covariance matrix (Eq. (29)). The choice of this constraint is consistent with assumption of an angularly homogeneous atmosphere. This climatology is mapped from the original 85 level pressure grid to retrieval levels using a least-squares estimate of the inverse of the single profile map from Eq. (34). The constraint vector, $\mathbf{x}_c$, is the same constraint vector used for the 2D retrieval.

6.3. Results for 1D retrieval

The 1D retrieval is computed in a similar manner as the 2D retrieval (see Section 5.4) where the map is from Eq. (47), the gain matrix (Eq. (20)) is computed with the Jacobian from Eq. (46) and the constraint is described in Section 6.2. The linear 1D retrieval results in 12 identical profiles. For comparison with the 2D retrieval, these 12 profiles are shown as an image in Fig. 5d. The retrieved profile suggests that the 1D limb retrieval also infers enhanced CO concentrations related to the plume above 7 km but no information about their angular variations. Consequently, the 1D retrieval maps this vertical estimate over the entire TES field-of-view.

Although a single profile is inferred for this 1D retrieval, the averaging kernel matrix is computed for the 2D atmosphere using Eq. (23) in order to show the sensitivity of the 1D retrieval to the two-dimensional distribution of CO. For comparison with the 2D retrieval, the diagonal of the averaging kernel matrix is shown in Fig. 6b. Like the 2D retrieval, the 1D retrieval is most sensitive to the cross section of CO between 6 and 13 km and between 3° and 5° latitude from the reference.

7. Comparison between 1D limb and 2D retrieval

The size of the averaging kernel and error covariance matrices makes comparisons between the 1D and 2D retrievals challenging. The degrees of freedom and information content are two metrics that reduce the averaging kernel and error covariance matrices, respectively, into scalar values that facilitate the comparison between two retrievals that are evaluated on the same full-state grid.

The DOFS, which is defined in Eq. (24), is a description of the number of independent pieces of information that can be inferred from a retrieval. Table 1 lists DOFS for the 1D and 2D retrieval. For the 2D retrieval, the DOFS is 7.1. The DOFS is distributed through the total number of state elements, which is 85 pressure levels $\times$ 12 angles $=$ 1020 elements. However, inspection of the diagonal of the averaging kernel in Fig. 6a indicates that the DOFS are concentrated over a cross-section of the full state vector. For the 1D retrieval, the DOFS is 3.1. This reduction in DOFS is consistent with the loss of angular resolution imposed by assuming the hard constraint of an angularly homogeneous atmosphere (Eq. (45)).

The information content, which is defined in Eq. (32), describes the relative change in volume between the retrieval error covariance and the a priori covariance matrix. Table 1 lists the information content of the 1D and 2D retrievals. As discussed in Section 4, this form of the information content

Table 1
Retrieval characterization

Retrieval	Constraint	DOF	Information content (bits)
2D	Mapped 2D S_a	7.2	9.8
1D	1D S_a	3.1	0.5

The first column is the retrieval type, the second column describes the constraint used for the retrieval. The DOF refers to the degrees of freedom for the retrieval. The information content describes the change in error volume as computed from the a priori and retrieval covariances. Every bit implies that the error volume of the retrieval is a factor of 2 less than the a priori covariance.

is given in "bits" with every bit implying that the error volume, relative to the a priori covariance, has been reduced by a factor of 2. The information content for the 2D retrieval is 9.8 bits whereas the information content for the 1D retrieval is 0.5 bits. This significant difference in information content between the 1D and 2D retrievals can be explained by the hard constraint in the 1D retrieval that forces the profile to be the same over all angles. Consequently, the smoothing and measurement covariance (Eq. (26)) can be larger than the a priori covariance in the cross section of CO where the retrieval is insensitive, as shown in Figs. 7b and c. On the other hand, the 2D retrieval is constrained to the a priori in the cross-section of CO where the retrieval is insensitive. Therefore, the 2D retrieval provides a net information gain in regions where the retrieval is sensitive but no information loss where the retrieval is insensitive.

8. Validation of limb retrieval

In situ and limb remote sensing measurements provide complementary information about the atmosphere. However, comparisons can be difficult between these measurements because of their differing spatial resolution [23]. These comparisons are often performed by directly examining the difference between an in situ measurement and the retrieved atmospheric profile from the sounder. The in situ profile and the retrieved profile are considered to be in "good" agreement if that difference is within the "error bars", i.e., the diagonal of the error covariance matrix, of the retrieval. Disagreement between profiles measured from the in situ and limb sounder may be attributed to inhomogeneity of the atmospheric constituents, instrument errors, or the differences in spatial resolution between the limb sounder and the in situ measurement.

The 2D characterization of the limb retrieval provides a framework that can be used to intercompare limb sounders with in situ measurements taken within the field-of-view of the sounder. This framework accounts for an inhomogeneous distribution of atmospheric constituents and differing spatial resolutions between in situ and limb retrieval measurements. As an example, we consider the intercomparison of the 1D CO limb retrieval with in situ measurements placed at different angles within the TES FOV. An in situ measurement of CO at 0° is a natural choice for an intercomparison because the CO amounts seen by the satellite in the layers at 0° are the largest relative to the CO amounts at the other angles. This approach has been used to intercompare in situ measurements with solar occultation measurements [21,24,25]. Nevertheless, a direct comparison of the profile at 0° to the 1D estimate would suggest that there was significant disagreement between the in situ measurement and the 1D retrieval. This disagreement is due in part to the effects of the constraints used in the retrieval. These effects can be accounted for by assuming that the in situ measurement is of an angularly homogeneous atmosphere. The profile from the in situ measurement is mapped to an angularly homogeneous atmosphere and substituted for the true full-state vector in Eq. (19). The simulated 1D limb retrieval for this angularly homogeneous atmosphere is shown in Fig. 9. The shape of the simulated 1D limb retrieval is similar to the 1D limb retrieval in Fig. 9 but there is still a significant discrepancy between magnitudes of the volume mixing ratio of the retrieved profile. This discrepancy can be explained in part by examining the averaging kernel of the 1D retrieval (Fig. 6b), which indicates that the limb retrieval is primarily sensitive to CO concentrations between 3° and 5° from the reference. Therefore, we can conclude that an intercomparsion of an in situ measurement at the 0° reference latitude and this limb retrieval is not useful.

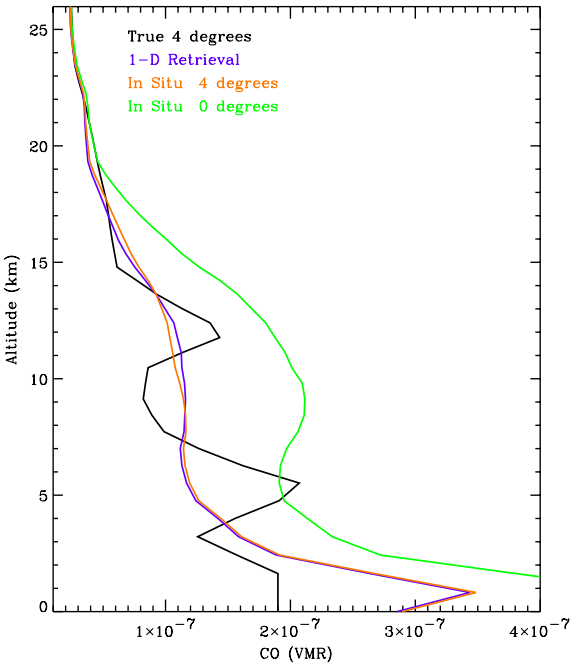

Fig. 9. The black line is the GEOS-CHEM vertical CO profile 4° from our reference latitude of 30N 140E. The blue line shows the results of the 1D limb retrieval. The green line shows a linear 1D retrieval where the true state over all angles is taken to be an in situ measurement at the reference latitude. The orange line shows a linear 1D retrieval where the true state over all angles is taken to be an in situ measurement at 4° from the reference latitude.

However, the averaging kernel can be used to determine where an in situ measurement should be placed in order to improve the intercomparison. From Fig. 6b, the sensitivity of the 1D limb retrieval peaks at 4°. Therefore, we consider the intercomparison of a in situ measurement placed at 4° with the 1D limb retrieval. The profile from the in situ measurement at 4° is mapped to an angularly homogeneous atmosphere and substituted for the true full-state vector in Eq. (19). The simulated 1D limb retrieval from the in situ measurement and the 1D limb retrieval of the angularly inhomogeneous 1D limb retrieval are shown in Fig. 9. The intercomparison shows a disagreement in the retrievals of no greater than 10 ppb of CO from 0 to 25 km. In this case, the 2D characterization of the 1D limb retrieval allowed for a more optimal placement of the in situ measurement for validation of the CO limb retrieval. Unfortunately, comparison of a single in situ measurement with a 1D limb retrieval provides little information about the angular distribution of the CO plume. However, this technique could be extended to a comparison of the 2D limb retrieval with multiple in situ measurements.

9. Summary and conclusions

In this paper we performed and characterized 1D and 2D limb retrievals of an atmosphere with an angular and radial distribution of carbon monoxide. For a test case, we chose a simulated

cross section of a CO plume off the coast of Japan. This cross section is located at 140° longitude and between 30° latitude and 40° latitude. We describe a model that calculates the angular radiance field measured by a limb sounder for a distribution of CO defined on a radial and angular grid. Based on this model, we calculate linear 1D and 2D limb retrievals of the CO plume.

Characterization of the 2D retrieval involved the calculation and interpretation of the 2D averaging kernel and error covariance on the radial and angular grid. From the averaging kernel, we find the retrievals to be most sensitive to the cross section of CO between 2° and 5° in front of the reference profile located at 140° longitude and 30° latitude even though the largest column amounts of CO along the line of sight of the instrument are between 0° and 2°. The 2D averaging kernel was also used to define a radial and angular resolution for the 2D retrieval. For regions where the retrieval was most sensitive, the resolution was about 7 km and 1.3°. Based on this resolution, we examined the columns of the profiles that span the CO plume as well as their corresponding estimates from the 2D retrieval. The estimated columns are accurate to within about 10% between 2° and 5° from the reference profile, which is sufficient to capture the angular variation of the corresponding columns of the CO plume.

In order to compare the 1D and 2D limb retrievals, the 1D limb retrieval is also characterized in two dimensions. We find the 1D retrieval is also most sensitive to the same cross section of CO as the 2D retrieval. Two metrics for these retrievals are also computed: the degrees of freedom for signal DOFS and the information content. The DOFS for the 2D retrieval is 7.2 versus 3.1 for the 1D retrieval. This reduction in DOFS is consistent with the loss of angular resolution imposed by assuming the hard constraint of an angularly homogeneous atmosphere. The information content for the 2D retrieval is 9.8 bits whereas the information content for the 1D retrieval is 0.5 bits. This significant difference in information content between the 1D and 2D retrievals was explained by the hard constraint in the 1D retrieval that forced the profile to be the same over all angles. Consequently, the total error covariance can be larger than the a priori covariance in the cross section of CO where the retrieval is insensitive. On the other hand, the 2D retrieval is constrained to the a priori in the cross-section of CO where the retrieval is insensitive. Therefore, the 2D retrieval provides a net information gain in regions where the retrieval is sensitive but no information loss where the retrieval is insensitive.

2D characterization also provides a means of comparing limb retrievals to one or more in situ measurements. As an example, we showed a comparison between the 1D limb retrieval and a single in situ measurement. The 2D averaging kernel was used to determine the best placement of the in situ measurement for comparison with the 1D limb retrieval.

Acknowledgements

We would like to thank the following people for their suggestions, discussions, and contributions to this research: Susan Sund, Clive Rodgers, Bashwar Sen, Reinhard Beer, Nathanial Livesey, Daniel Jacob, Helen Worden, and Tony Clough. The research described in this paper was performed at the Jet Propulsion Laboratory, California Institute of Technology, under a contract with the National Aeronautics and Space Administration.

References

[1] Pan LW, Gille JC, Edwards DP, Bailey PL, Rodgers CD. Retrieval of tropospheric carbon monoxide for the MOPITT experiment. J Geophys Res—Atmos 1998;103(D24):32277–90.
[2] Bowman KW, Worden J, Steck T, Worden HM, Clough S, Rodgers CD. Capturing time and vertical variability of tropospheric ozone: a study using TES nadir retrievals 2002;107(23):4723.
[3] Toon GC, Blavier JF, Sen B, Margitan JJ, Webster CR, May RD, Fahey D, Gao R, Del Negro L, Proffitt M, Elkins J, Romashkin PA, Hurst DF, Oltmans S, Atlas E, Schauffler S, Flocke F, Bui TP, Stimpfle RM, Bonne GP, Voss PB, Cohen RC. Comparison of MkIV balloon and ER-2 aircraft measurements of atmospheric trace gases. J Geophys Res—Atmos 1999;104(D21):26779–90.
[4] Stiller GP, von Clarmann T, Funke B, Glatthor N, Hase F, Hopfner M, Linden A. Sensitivity of trace gas abundances retrievals from infrared limb emission spectra to simplifying approximations in radiative transfer modelling. JQSRT 2002;72(3):249–80.
[5] Ridolfi M, Carli B, Carlotti M, von Clarmann T, Dinelli BM, Dudhia A, Flaud JM, Hopfner M, Morris PE, Raspollini P, Stiller G, Wells RJ. Optimized forward model and retrieval scheme for MIPAS near- real-time data processing. Appl Opt 2000;39(8):1323–40.
[6] Livesey NJ, Read WG. Direct retrieval of line-of-sight atmospheric structure from limb sounding observations. Geophys Res Lett 2000;27(6):891–4.
[7] Bey I, Jacob DJ, Yantosca RM, Logan JA, Field BD, Fiore AM, Li QB, Liu HGY, Mickley LJ, Schultz MG. Global modeling of tropospheric chemistry with assimilated meteorology: model description and evaluation. J Geophys Res—Atmos 2001;106(D19):23073–95.
[8] Schneider HR, Jones DBA, McElroy MB, Shi GY. Analysis of residual mean transport in the stratosphere 1. Model description and comparison with satellite data. J Geophys Res—Atmos 2000;105(D15):19991–20011.
[9] McLinden CA, Olsen SC, Hannegan B, Wild O, Prather MJ, Sundet J. Stratospheric ozone in 3-D models: a simple chemistry and the cross-tropopause flux. J Geophys Res—Atmos 2000;105(D11):14653–65.
[10] Beer R, Glavich TA, Rider DM. Tropospheric emission spectrometer for the Earth Observing System's Aura Satellite. Appl Optics 2001;40(15):2356–67.
[11] Clough SA, Worden JR, Brown PD, Shephard MW, Rinsland CP, Beer R. Retrieval of tropospheric ozone from simulations of limb spectral radiances as observed from space 2002;107(D21):4589.
[12] Clough SA, Iacono MJ. Line-by-line calculation of atmospheric fluxes and cooling rates 2. Application to carbon-dioxide, ozone, methane, nitrous-oxide and the halocarbons. J Geophys Res—Atmos 1995;100(D8):16519–35.
[13] Clough SA, Iacono MJ, Moncet JL. Line-by-line calculations of atmospheric fluxes and cooling rates—application to water-vapor. J Geophys Res—Atmos 1992;97(D14):15761–85.
[14] Rodgers CD. Inverse methods for atmospheric sounding: theory and practice. Singapore: World Scientific Computing Co.; 2000.
[15] Marks CJ, Rodgers CD. A retrieval method for atmospheric composition from limb emission measurements. J Geophys Res—Atmos 1993;98(D8):14939–53.
[16] Papoulis A. Probability, random variables and stochastic processes. New York: McGraw-Hill; 1984.
[17] Conrath BJ. Vertical resolution of temperature profiles obtained form remote radiation measurements. J Atmos Sci 1972;29(7):1262.
[18] Fishbein EF, Cofield RE, Froidevaux L, Jarnot RF, Lungu T, Read WG, Shippony Z, Waters JW, McDermid IS, McGee TJ, Singh U, Gross M, Hauchecorne A, Keckhut P, Gelman ME, Nagatani RM. Validation of UARS microwave limb sounder temperature and pressure measurements. J Geophys Res—Atmos 1996;101(D6):9983–10016.
[19] Sen B, Toon GC, Osterman GB, Blavier JF, Margitan JJ, Salawitch RJ, Yue GK. Measurements of reactive nitrogen in the stratosphere. J Geophys Res—Atmos 1998;103(D3):3571–85.
[20] Irion FW, Gunson MR, Toon GC, Chang AY, Eldering A, Mahieu E, Manney GL, Michelsen HA, Moyer EJ, Newchurch MJ, Osterman GB, Rinsland CP, Salawitch RJ, Sen B, Yung YL, Zander R. Atmospheric trace molecule spectroscopy (ATMOS) experiment version 3 data retrievals. Appl Opt 2002;41(33):6968–79.
[21] Toon GC, Blavier JF, Sen B, Margitan JJ, Webster CR, May RD, Fahey D, Gao R, Del Negro L, Proffitt M, Elkins J, Romashkin PA, Hurst DF, Oltmans S, Atlas E, Schauffler S, Flocke F, Bui TP, Stimpfle RM, Bonne GP, Voss PB,

Cohen RC. Comparison of MkIV balloon and ER-2 aircraft measurements of atmospheric trace gases. J Geophys Res—Atmos 1999;104(D21):26779–90.
[22] Wayne RP. Chemistry of atmosphere, 2nd ed. Oxford: Oxford University Press; 1991.
[23] Rodgers CD, Connor BJ. Intercomparison of remote sounding instruments. J Geophys Res—Atmos 2003;108(D3):2299.
[24] Chang AY, Salawitch RJ, Michelsen HA, Gunson MR, Abrams MC, Zander R, Rinsland CP, Loewenstein M, Podolske JR, Proffitt MH, Margitan JJ, Fahey DW, Gao RS, Kelly KK, Elkins JW, Webster CR, May RD, Chan KR, Abbas MM, Goldman A, Irion FW, Manney GL, Newchurch MJ, Stiller GP. A comparison of measurements from ATMOS and instruments aboard the ER-2 aircraft: tracers of atmospheric transport. Geophys Res Lett 1996;23(17):2389–92.
[25] Lumpe JD, et al. Comparison of POAM III ozone measurements with correlative aircraft and balloon data during SOLVE. J Geophys Res 2002;107:8316.